Eur. Phys. J. C (2017) 77:94
DOI 10.1140/epjc/s10052-017-4660-9

THE EUROPEAN PHYSICAL JOURNAL C

Regular Article - Theoretical Physics

$B_s\pi - B\bar{K}$ interactions in finite volume and $X(5568)$

Jun-Xu Lu[1], **Xiu-Lei Ren**[2], **Li-Sheng Geng**[1,a]

[1] School of Physics and Nuclear Energy Engineering, International Research Center for Nuclei and Particles in the Cosmos, Beijing Key Laboratory of Advanced Nuclear Materials and Physics, Beihang University, Beijing 100191, China
[2] State Key Laboratory of Nuclear Physics and Technology, School of Physics, Peking University, Beijing 100871, China

Received: 6 October 2016 / Accepted: 30 January 2017 / Published online: 13 February 2017

Abstract The recent observation of $X(5568)$ by the D0 Collaboration has aroused a lot of interest both theoretically and experimentally. In the present work, we first point out that $X(5568)$ and $D_{s0}^*(2317)$ cannot simultaneously be of molecular nature, from the perspective of heavy-quark symmetry and chiral symmetry, based on a previous study of the lattice QCD scattering lengths of DK and its coupled channels. Then we compute the discrete energy levels of the $B_s\pi$ and $B\bar{K}$ system in finite volume using unitary chiral perturbation theory. The comparison with the latest lattice QCD simulation, which disfavors the existence of $X(5568)$, supports our picture where the $B_s\pi$ and $B\bar{K}$ interactions are weak and $X(5568)$ cannot be a $B_s\pi$ and $B\bar{K}$ molecular state. In addition, we show that the extended Weinberg compositeness condition also indicates that $X(5568)$ cannot be a molecular state made from $B_s\pi$ and $B\bar{K}$ interactions.

1 Introduction

Recently, an apparently exotic mesonic state, the so-called $X(5568)$ state, was observed by the D0 Collaboration in the $B_s^0\pi^\pm$ invariant mass spectrum [1]. The extracted mass and width are $M = 5567.8 \pm 2.9^{+0.9}_{-1.9}$ MeV and $\Gamma = 21.9 \pm 6.4^{+5.0}_{-2.5}$ MeV, respectively, and the preferred spin-parity is $J^P = 0^+$. This state, being one of the exotic XYZ states [2], should contain at least four valence quark flavors u, d, s, and b.

The experimental observation of $X(5568)$ has inspired much theoretical work. It has been proposed to be either a tetraquark state [3–14], a triangular singularity [15], or a molecular state [16]. Although these theoretical studies favor the existence of a state that can be identified as the $X(5568)$, some other studies have yielded negative conclusions. For instance, the difficulty to accommodate such a narrow structure with a relatively low mass has been stressed by Burns et al. [17] and Guo et al. [18]. A recent study in the chiral quark model showed that neither diquark–antidiquark nor meson–meson structures support the existence of $X(5568)$ [19]. In Ref. [20], the lowest-lying tetraquark s-wave state was found to be 150 MeV higher than $X(5568)$. On the experimental side, neither the LHCb nor the CMS Collaboration found a signal corresponding to $X(5568)$ [21,22].

Approximate heavy-quark symmetry and its breaking pattern provide a powerful tool to understand the nature of $X(5568)$. In the charm sector, $D_{s0}^*(2317)$ has been suggested to be a molecular state made from DK and $D_s\eta$ interactions in many studies; see, e.g., Refs. [23–28].[1] Naively, $X(5568)$ might be a heavy-quark partner of the $D_{s0}^*(2317)$. However, in Ref. [18], the authors point out that if one assumes a molecular picture for the $X(5568)$, heavy-quark symmetry then dictates that the charmed partner of $X(5568)$ should be located around 2.24 ± 0.15 GeV. So far, no signal has been reported yet with the associated quantum numbers in this energy region [18]. Note that the QCD sum rules predicted that the charmed partner of $X(5568)$ is located at much higher energies about 2.5–2.6 GeV [4,29].

The unitary chiral perturbation theory (UChPT), respecting both approximate heavy-quark symmetry and chiral symmetry and their breaking pattern, has turned out to be a useful tool in understanding the XYZ states. In Ref. [28], using the lattice QCD (lQCD) scattering lengths [27] to fix the relevant low energy constants (LECs) of the covariant UChPT, one found that the $D_{s0}^*(2317)$ emerges naturally, similar to Refs. [27,30,31]. When extended to the bottom sector guided by heavy-quark symmetry, the covariant UChPT shows that the interactions in the $B_s\pi - B\bar{K}$ channel are rather weak and do not support the existence of a low-lying resonance or bound state, consistent with an explicit search on the second Riemann sheet [28].

[a] e-mail: lisheng.geng@buaa.edu.cn

[1] In Refs. [23–26,28], the bottom parter of $D_{s0}^*(2317)$ was also predicted.

Nevertheless, in Ref. [32], the authors performed a fit to the D0 invariant mass distribution [1] by employing the $B_s\pi$ and $B\bar{K}$ coupled channel unitary chiral amplitudes and treating the unknown subtraction constant as a free parameter. The best fit yields a dynamically generated state consistent with $X(5568)$ [1]. Nevertheless, the authors noted that a large cutoff Λ, compared with a "natural" size of about 1 GeV, is needed to describe the D0 data. The unusual size of the cutoff points clearly to the presence of missing channels, contributions of other sources, or existence of "non-molecular" components, such as sizable tetraquark configurations, in the framework of the UChPT. As a result, it was concluded that a pure molecular state, dynamically generated by the unitary loops, is disfavored. A similar conclusion was reached in a later study utilizing p-wave coupled channel dynamics in the UChPT [33]. It should be pointed out that irrespective of the nature of $X(5568)$, the UChPT of Ref. [32] provides a good description of the D0 data. Therefore, it needs to be further tested.

In the present work, we would like to formulate the UChPT of Refs. [28,32] in finite volume and compute relevant discrete energy levels and scattering lengths. A comparison with lattice QCD simulations then allows one to distinguish these two scenarios and provides more clues about the nature of the $X(5568)$. In the remaining of this paper, we denote the UChPT of Ref. [32] by X-UChPT and that of Ref. [28] by $\not{X}$-UChPT to indicate that one of them dynamically generates $X(5568)$ and the other does not.

This paper is organized as follows. In Sect. 2, we briefly describe the UChPT of Ref. [28] and Ref. [32] and then in Sect. 3 we point out that from the perspective of heavy-quark symmetry and chiral symmetry as implemented in UChPT, the lQCD scattering lengths of DK and its coupled channels imply that the $B_s\pi$ and $B\bar{K}$ interactions are rather weak and do not support a molecular state that can be identified as $X(5568)$. As a result, a typical molecular picture for $X(5568)$ similar to that for the $D_{s0}^*(2317)$ case is not favored in UChPT, which is supported by the extended Weinberg compositeness condition. In Sect. 4, we formulate the UChPT of Refs. [28,32] in a finite box and calculate the discrete energy levels that can be extracted in a lattice QCD simulation. The results are contrasted with the latest lQCD simulation of Ref. [34], followed by a short summary in Sect. 5.

2 Unitary chiral perturbation theory

UChPT has two basic building blocks, a kernel potential provided by chiral perturbation theory and a unitarization procedure. The kernel potentials constrained by chiral symmetry and other relevant symmetries, such as heavy-quark symmetry in the present case, are standard in most cases, while the unitarization procedures can differ in their treatment of left-hand cuts or higher order effects, although they all satisfy two-body elastic unitarity.

The leading order kernel potential employed in Refs. [28, 32] has the following form:

$$V_{ij} = \frac{C_{ij}}{8f^2}\left(3s - (M_i^2 + m_i^2 + M_j^2 + m_j^2) - \frac{\Delta_1\Delta_2}{s}\right), \quad (1)$$

where $i = 1(2)$ denotes the $B_s\pi$ ($B\bar{K}$) channel, s is the invariant mass squared of the system, f is the pseudoscalar meson decay constant in the chiral limit, $\Delta_i = M_i^2 - m_i^2$ and $M_1(m_1)$ and $M_2(m_2)$ are the masses of $B_s(\pi)$ and $B(\bar{K})$ mesons. The coefficients C_{ij} are $C_{11} = C_{22} = 0$, $C_{12} = C_{21} = 1$.

In Refs. [28,32], the Bethe–Salpeter equation is adopted to unitarize the chiral kernel obtained above. In the context of the UChPT, the integral Bethe–Salpeter equation is often simplified and approximated as an algebraic equation with the use of the on-shell approximation.[2] It reads

$$T = V + VGT, \quad (2)$$

where T is the unitarized amplitude, V the potential, and G the one-loop 2-point scalar function. In n dimensions, G has the following simple form:

$$G_i = i\int \frac{\mathrm{d}^n q}{(2\pi)^n}\frac{1}{[(P-q)^2 - m_i + i\epsilon][q^2 - M_i^2 + i\epsilon]}, \quad (3)$$

where P is the total center-of-mass momentum of the system.

The loop function G is divergent and needs to be regularized. In the dimensional regularization scheme, it has the following form:

$$\begin{aligned} G_{\overline{\mathrm{MS}}}(s, M^2, m^2) = \frac{1}{16\pi^2}\Bigg[&\frac{m^2 - M^2 + s}{2s}\log\left(\frac{m^2}{M^2}\right) \\ &- \frac{q}{\sqrt{s}}(\log[2q\sqrt{s} + m^2 - M^2 - s] \\ &+ \log[2q\sqrt{s} - m^2 + M^2 - s] \\ &- \log[2q\sqrt{s} + m^2 - M^2 + s] \\ &- \log[2q\sqrt{s} - m^2 + M^2 + s]) \\ &+ \left(\log\left(\frac{M^2}{\mu^2}\right) + a\right)\Bigg], \end{aligned} \quad (4)$$

where a is the subtraction constant, and μ the regularization scale and $s = P^2$. The difference between Eq. (4) and its counterpart in Ref. [32] is a constant and can be absorbed into the subtraction constant.

It has been noted that the relativistic loop function, Eq. (4), violates heavy-quark symmetry and the naive chiral power counting. Several methods (see, e.g., Refs. [24,26,36,37])

[2] For a recent study of off-shell effects, see Ref. [35] and the references cited therein.

have been proposed to deal with such a problem. In $\not{X}$-UChPT [28], the minimal subtraction scheme is modified to explicitly conserve heavy quark symmetry and the naive chiral power counting. Confined to either the charm sector or the bottom sector alone, the modified subtraction scheme, termed the heavy-quark-symmetry (HQS) inspired scheme, is equivalent to the $\overline{\text{MS}}$ scheme, but it can link both sectors in a way that conserves heavy-quark symmetry up to order $1/M_H$, with M_H the chiral limit of the heavy hadron mass.[3] The loop function of the HQS scheme is related with that of the $\overline{\text{MS}}$ scheme via

$$G_{\text{HQS}} = G_{\overline{\text{MS}}} - \frac{1}{16\pi^2}\left(\log\left(\frac{\mathring{M}^2}{\mu^2}\right) - 2\right) + \frac{m_{\text{sub}}}{16\pi^2 \mathring{M}}\left(\log\left(\frac{\mathring{M}^2}{\mu^2}\right) + a'\right), \tag{5}$$

where m_{sub} is the average mass of the Goldstone bosons, $\mathring{M}$ the chiral limit value of the bottom (charm) meson masses and a' the subtraction constant. In the HQS scheme, the subtraction constant determined in the charm (bottom) sector is the same as that determined in the bottom (charm) sector, while this is not the case for the subtraction constant of the $\overline{\text{MS}}$ scheme. However, one may use the same cutoff in the cutoff scheme for both bottom and charm sectors related via heavy-quark symmetry (for a different argument, see, e.g., Ref. [39]).

In Ref. [28], it was shown that the LO potential of Eq. (1) cannot describe the lQCD scattering lengths of Ref. [27]. One needs go to the next-to-leading order (NLO). At NLO, there are six more LECs, namely c_0, c_1, c_{24}, c_{35}, c_4, c_5. Among them, c_0 is determined by fitting to the light quark mass dependence of lQCD D and D_s masses [27], and c_1 is determined by reproducing the experimental D and D_s mass difference. Once c_0 and c_1 are fixed, the remaining LECs and the subtraction constant are determined by fitting to the lQCD scattering lengths of Ref. [27], yielding a $\chi^2/\text{d.o.f.} = 1.23$. With these LECs, $D^*_{s0}(2317)$ appears naturally at 2317 ± 10 MeV. As a result, in the present work we employ the NLO UChPT of Ref. [28].

3 Scattering lengths and compositeness

3.1 Scattering lengths

The scattering lengths of a D (D_s) meson with a Nambu–Goldstone pseudoscalar meson have been studied on a lattice [27]. With these scattering lengths as inputs, various groups have predicted the existence of $D^*_{s0}(2317)$ and its counterparts both in the charm sector and in the bottom sector [28,30,31]. It is worth pointing out that the predicted counterparts of the $D^*_{s0}(2317)$ and $D_{s1}(2416)$ are indeed observed in a later lQCD simulation [40]. In the following, we compare the scattering lengths of $B_s\pi$, $B\bar{K}$, $D_s\pi$, and DK obtained in $\not{X}$-UChPT [28] with those obtained in X-UChPT [32], to check the consistency between the constraint imposed by the existence of the $X(5568)$ and that of $D^*_{s0}(2317)$ and the lQCD scattering lengths of Ref. [27].

The scattering length of channel i is defined as

$$a_{ii} = -\frac{1}{8\pi(M_i + m_i)} T_{ii}(s = (M_i + m_i)^2). \tag{6}$$

Using the G function determined in Ref. [28] and Ref. [32],[4] we obtain the scattering lengths of $B\bar{K}$ and $B_s\pi$ tabulated in Table 1. Clearly, the results obtained in the two approaches are quite different. The scattering lengths, particularly that of $B_s\pi$ obtained in $\not{X}$-UChPT [28], show clearly that the interactions are rather weak in the $B_s\pi$ and $B\bar{K}$ coupled channels. This implies that there is no bound state or resonant state, consistent with a direct search on the second Riemann sheet. For the sake of comparison, Table 1 also lists the scattering lengths of DK and $D_s\pi$. We note that the scattering lengths obtained in X-UChPT [32] are much larger than those of $\not{X}$-UChPT [28], inconsistent with the lQCD results of Ref. [27].

lQCD simulations allow one to understand more physical observables by studying their quark mass dependence. In this regard, it is useful to study the m_π dependence of the scattering lengths. For such a purpose in the UChPT, one needs the pion mass dependence of the constituent hadrons, namely, m_K, m_B and m_{B_s}. Following Ref. [28], we take

$$\begin{aligned} m_K^2 &= \hat{a} + \hat{b} m_\pi^2, \\ m_B^2 &= m_0^2 + 4c_0(m_\pi^2 + m_K^2) - 4c_1 m_\pi^2, \\ m_{B_s}^2 &= m_0^2 + 4c_0(m_\pi^2 + m_K^2) + 4c_1(m_\pi^2 - 2m_K^2), \end{aligned} \tag{7}$$

with $\hat{a} = 0.317$, $\hat{b} = 0.487$, $c_0 = 0.015$, and $c_1 = -0.513$. These LECs are fixed using the experimental data and the lattice QCD masses of Ref. [27] as explained above.

In Fig. 1, we show the scattering lengths $a_{B_s\pi}$ and $a_{B\bar{K}}$ as a function of the pion mass. One can see that $a_{B_s\pi}$ shows some "threshold" effects. These effects can easily be understood from the amplitude expressed in terms of couplings and pole positions,

$$T_{ii}(s) = \frac{g_i^2}{\sqrt{s} - \sqrt{s}_0}, \tag{8}$$

where g_i is the coupling defined in Eq. (10), and $\sqrt{s}_0$ the pole position. To calculate the scattering lengths, $\sqrt{s} = m_{B_s} + m_\pi$. Once the trajectory of the threshold crosses that of the

[3] For an application of the HQS scheme in the singly charmed (bottom) baryon sector, see Ref. [38].

[4] The loop function is always regularized in the dimensional regularization scheme, unless otherwise specified.

Table 1 $B_s\pi$, $B\bar{K}$, $D_s\pi$, and DK scattering lengths in $\not{X}$-UChPT [28] and X-UChPT [32][a], in units of fm

Coupled channels	$\not{X}$-UChPT [28]	X-UChPT [32]	Coupled channels	$\not{X}$-UChPT [28]	X-UChPT [32]
$B\bar{K}$	$0.020 - 0.231i$	$-0.194 - 0.014i$	DK	$0.056 - 0.158i$	$-0.253 - 0.038i$
$B_s\pi$	-0.006	0.206	$D_s\pi$	0.004	0.126

[a] For X-UChPT [32], the scattering lengths are calculated using the loop function regularized in the cutoff scheme with the cutoff fixed by fitting to the D0 data. See Sect. 2 for details

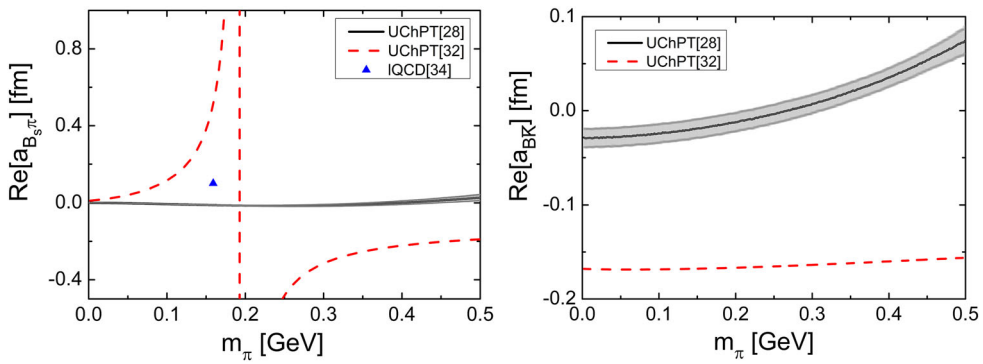

Fig. 1 Real part of the scattering lengths $a_{B_s\pi}$ and $a_{B\bar{K}}$ as a function of the pion mass m_π obtained in $\not{X}$-UChPT [28] and X-UChPT [32]. The *uptriangle* in the *left panel* denotes the lQCD result of Ref. [34], which is an average of the six data obtained using different sets of gauge configurations (see the bottom panel of Fig. 2 of Ref. [34]). The *shaded area* indicates uncertainties originating from the lQCD data of Ref. [27]

pole as m_π varies, a singularity will emerge. In fact, similar effects have already been observed in Ref. [41]. On the other hand, as m_π increases, $a_{B\bar{K}}$ stays more or less constant in X-UChPT [32], while it increases slightly in $\not{X}$-UChPT [28]. For the sake of comparison, we also show the lQCD result of Ref. [34]. We note that the lQCD result, obtained with a π mass close to its physical value, lies in between the results of Refs. [28,32], and thus cannot distinguish the two scenarios. For such a purpose, lQCD simulations with quark masses larger than their physical values will be more useful.

3.2 Compositeness of $X(5568)$

The large cutoff used in X-UChPT [32] indicates that the dynamically generated $X(5568)$ should contain rather large non-$B_s\pi$ and $B\bar{K}$ components. This can be quantified using the Weinberg composition condition and its extensions [42–58].

Following Ref. [51] we define the weight of a hadron–hadron component in a composite particle by

$$X_i = -\mathrm{Re}\left[g_i^2 \left[\frac{\partial G_i^{\mathrm{II}}(s)}{\partial \sqrt{s}} \right]_{\sqrt{s}=\sqrt{s_0}} \right], \tag{9}$$

where $\sqrt{s_0}$ is the pole position, G_i^{II} is the loop function evaluated on the second Riemann sheet, and g_i is the coupling of the respective resonance or bound state to channel i calculated as

$$g_i^2 = \lim_{\sqrt{s}\to\sqrt{s_0}} (\sqrt{s} - \sqrt{s_0}) T_{ii}^{\mathrm{II}}, \tag{10}$$

where T_{ii}^{II} is the ii element of the T amplitude on the second Riemann sheet.

The deviation of the sum of X_i from unity is related to the energy dependence of the s-wave potential,

$$\sum_i X_i = 1 - Z, \tag{11}$$

where

$$Z = -\sum_{ij} \left[g_i G_i^{\mathrm{II}}(\sqrt{s}) \frac{\partial V_{ij}(\sqrt{s})}{\partial \sqrt{s}} G_j^{\mathrm{II}}(\sqrt{s}) g_j \right]_{\sqrt{s}=\sqrt{s_0}}. \tag{12}$$

The quantity Z is often attributed to the weight of missing channels.

Using X-UChPT [32], we obtain $X_{B\bar{K}} = 0.10 - 0.02i$, $X_{B_s\pi} = 0.06 + 0.11i$, and $Z = 0.83 - 0.09i$. The value of Z is much larger than the typical size for a state dominated by molecular components, which indicates the missing of contributions of other components. Such a result is consistent with the unusual size of Λ and similar conclusions have been drawn in Ref. [32].

One should note that the above defined compositeness and the so-drawn conclusion are model dependent, which is different from the original Weinberg criterion. In this formalism, the compositeness and elementariness are defined as the fractions of the contributions from the two-body scattering states and one-body bare states to the normalization of the total

wave function within the particular model space, respectively (see, e.g., Ref. [55]). In the present case, the small compositeness $1-Z$ simply indicates that in the model space of the $\not{X}$-UChPT [32], the meson–meson components only account for a small fraction of the total wave function, and thus $X(5568)$ cannot be categorized as a meson–meson molecule.

4 $B_s\pi$ and $B\bar{K}$ interactions in finite volume

If $X(5568)$ exists, one should be able to observe it in a lQCD simulation, which can be anticipated in the near future, given the fact that the LHCb result has cast doubts on the existence of the $X(5568)$. In view of such possibilities, in the following, we predict the discrete energy levels that one would obtain in a lattice QCD simulation. Such an exercise provides a highly non-trivial test of $\not{X}$-UChPT [28] and X-UChPT [32].

In this work, we follow the method proposed in Ref. [59] to calculate the loop function G in finite volume in the dimensional regularization scheme. Introducing a finite-volume correction, δG, $\tilde{G}$ can be written as

$$\tilde{G} = G^D + \delta G, \tag{13}$$

where G^D is the loop function calculated in the dimensional regularization scheme, either $G_{\rm HQS}$ or $G_{\overline{\rm MS}}$, and δG has the following form [59]:

$$\delta G = -\frac{1}{4}\int_0^1 {\rm d}x\,\delta_{3/2}(\mathcal{M}^2(s)), \tag{14}$$

where

$$\mathcal{M}^2(s) = (x^2-x)s + xM^2 + (1-x)m^2 - i\epsilon. \tag{15}$$

For the case of $\sqrt{s} > M+m$, $\delta_r(\mathcal{M}^2(s))$ can be written as a sum of the following three parts [60,61]:

$$\delta_r(\mathcal{M}^2(s)) = g_1^r - g_2^r + g_3^r, \tag{16}$$

where $g_{1,2,3}^r$ are

$$\begin{aligned}
g_1^r &= \frac{1}{L^3}\sum_{\vec{q}}\left\{\frac{1}{\left[\frac{4\pi^2\vec{n}^2}{L^2}+\mathcal{M}^2(s)\right]^r}\right.\\
&\left.-\frac{1}{\left[\frac{4\pi^2\vec{n}^2}{L^2}+\mathcal{M}^2(m_{ss}^2)\right]^r}+\frac{r(x^2-x)(s-m_{ss}^2)}{\left[\frac{4\pi^2\vec{n}^2}{L^2}+\mathcal{M}^2(m_{ss}^2)\right]^{r+1}}\right\},\\
g_2^r &= \int_0^{+\infty}\frac{q^2{\rm d}q}{2\pi^2}\left\{\frac{1}{[\vec{q}^2+\mathcal{M}^2(s)]^r}\right.\\
&\left.-\frac{1}{[\vec{q}^2+\mathcal{M}^2(m_{ss}^2)]^r}+\frac{r(x^2-x)(s-m_{ss}^2)}{[\vec{q}^2+\mathcal{M}^2(m_{ss}^2)]^{r+1}}\right\},\\
g_3^r &= \delta_r(\mathcal{M}^2(m_{ss}^2)) - r(x^2-x)(s-m_{ss}^2)\delta_{r+1}(\mathcal{M}^2(m_{ss}^2)),
\end{aligned} \tag{17}$$

and L is the spatial size of the lattice.[5] The separation scale m_{ss} needs to satisfy $m_{ss} < M+m$. In the case of $\sqrt{s} < M+m$, $\delta_r(\mathcal{M}^2(s))$ can be expressed as [62]

$$\begin{aligned}
\delta_r(\mathcal{M}^2(s)) = &\frac{2^{-1/2-r}(\sqrt{\mathcal{M}})^{3-2r}}{\pi^{3/2}\Gamma(r)}\\
&\times\sum_{\vec{n}\neq 0}(L\sqrt{\mathcal{M}^2}|\vec{n}|)^{-3/2+r}K_{3/2-r}(L\sqrt{\mathcal{M}^2}|\vec{n}|),
\end{aligned} \tag{18}$$

where $K_n(z)$ is the modified Bessel function of the second kind, and

$$\sum_{\vec{n}\neq 0} \equiv \sum_{n_x=-\infty}^{\infty}\sum_{n_y=-\infty}^{\infty}\sum_{n_z=-\infty}^{\infty}(1-\delta(|\vec{n}|,0)), \tag{19}$$

with $\vec{n} = (n_x, n_y, n_z)$. It should be mentioned that in actual calculations the discrete summations in Eqs. (17)–(19) are only taken up to a certain number, $|n|_{\rm max} = L/(2a)$ with a the lattice spacing.

The Bethe–Salpeter equation in finite volume reads

$$\tilde{T} = \frac{1}{V^{-1}-\tilde{G}}. \tag{20}$$

The discrete energy levels one would observe in a lattice QCD simulation are determined via $\det(V^{-1}-\tilde{G}) = 0$.

In Fig. 2, we show the so-obtained discrete energy levels in both scenarios, X-UChPT [32] and $\not{X}$-UChPT [28]. From the left panel, one can clearly identify an extra energy level, namely, the second energy level, which can be associated to $X(5568)$. All the other discrete energy levels lie close to one of the free energy levels, $B_s\pi(\ell)$ or $B\bar{K}(\ell)$, where ℓ denotes the energy of the corresponding discrete energy level with energy $E[B_s\pi(\ell)] = \sqrt{m_{B_s}^2+k^2}+\sqrt{m_\pi^2+k^2}$ wth $k = \ell\frac{2\pi}{L}$ ($\ell = 0, 1, 2, \ldots$) and likewise for $E[B\bar{K}(\ell)]$. On the other hand, no extra energy level appears in the right panel, consistent with the fact that the interactions are weak and no resonance or bound state is found in $\not{X}$-UChPT [28].

In a recent study [34], a lQCD simulation employing the PACS-CS gauge configurations was performed [63]. It was shown that no state corresponding to $X(5568)$ exists in the simulation, consistent with the LHCb result [21]. In addition, the authors of Ref. [34] provided an analytic prediction based on the Lüscher method. They included the $X(5568)$ explicitly via a resonant Breit–Wigner-type phase shift and then related the phase shift with the discrete energy levels through the Lüscher method. For more details we refer to subsection II.A of Ref. [34]. In Fig. 3, we compare the lQCD discrete energy levels with those obtained in our present study. Since

[5] Throughout this paper, we assume a periodic boundary condition for the lQCD setup and that the temporal size is much larger than the spatial size and therefore can be taken as infinity.

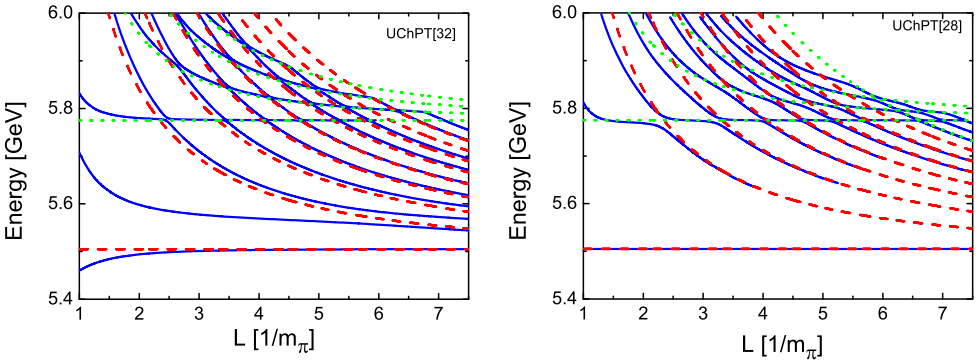

Fig. 2 Discrete energy levels of the $B_s\pi$–$B\bar{K}$ system as a function of the lattice size L. *Left panel* obtained with X-UChPT [32]; *right panel* obtained with $\not{X}$-UChPT [28]. The *solid lines* are the energy levels obtained by solving Eq. (20), while the *dashed* and *dotted lines* are the energy levels of non-interacting $B_s\pi$ and $B\bar{K}$ pairs, respectively

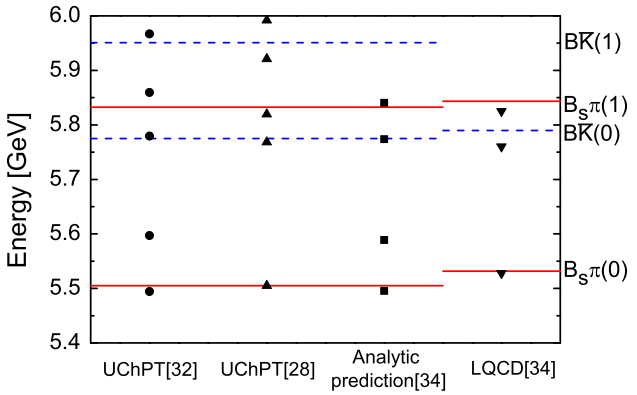

Fig. 3 Discrete energy levels at $L = 2.9$ fm obtained in different approaches: the *solid points*, *up triangles*, *squares*, and *down triangles* correspond to the results of X-UChPT [32], $\not{X}$-UChPT [28], the analytic prediction using the Lüscher method [34], and the lQCD results of Ref. [34], respectively. The *solid* (*dashed*) *lines* refer to the energy levels of non-interacting $B_s\pi$ ($B\bar{K}$) pairs

the quark masses in the lQCD simulation are not yet physical, the non-interacting energy levels of the lQCD are slightly shifted upward compared to those calculated theoretically using physical meson masses. Apparently, the lQCD results are consistent with $\not{X}$-UChPT [28], but not X-UChPT [32] in which a large cutoff was used to reproduce the D0 data. On the other hand, the analytic predictions based on the Lüscher method [34] are consistent with X-UChPT [32], as they should be since in Ref. [34], the D0 $X(5568)$ mass and width were employed in the Lüscher method as inputs and in Ref. [32] the only parameter in X-UChPT, the subtraction constant, was fixed by fitting to the D0 data. We should note that, for a single channel, the Lüscher method is consistent with the Jülich–Valencia approach adopted in the present work (see, e.g., Ref. [59] for an explicit comparison in the case of KK^* scattering).

From the above comparison, one can conclude that there is indeed a tension among the D0 data, the lQCD results of Ref. [34], and indirectly those of Ref. [27], provided that heavy-quark symmetry and chiral symmetry are not somehow strongly broken.

5 Summary

The recent D0 claim of the existence of $X(5568)$ has aroused a lot of interest. In the present paper, we showed explicitly the tension between the D0 discovery and the lQCD results on the charmed meson–pseudoscalar meson scattering, including the scattering lengths and the existence of $D_{s0}^*(2317)$, from the perspective of approximate chiral symmetry and heavy-quark symmetry as implemented in the unitary chiral perturbation theory. We then formulated the unitary chiral description of the coupled channel $B_s\pi$–$B\bar{K}$ interactions in finite volume. Our results, when compared with the latest lattice QCD simulation, confirm the inconsistency and disfavor the existence of $X(5568)$ in unitary chiral perturbation theory. We conclude that more experimental and theoretical efforts are needed to clarify the current situation.

Acknowledgements We thank Eulogio Oset for a careful reading of the first version of this manuscript and for his valuable comments. This work is partly supported by the National Natural Science Foundation of China under Grants Nos. 11375024, 11522539, 11335002, and 11411130147, the Fundamental Research Funds for the Central Universities, the Research Fund for the Doctoral Program of Higher Education under Grant No. 20110001110087, and the China Postdoctoral Science Foundation under Grant No. 2016M600845.

References

1. V.M. Abazov et al., D0 Collaboration, Phys. Rev. Lett. **117**, 022003 (2016). arXiv:1602.07588 [hep-ex]
2. H.X. Chen, W. Chen, X. Liu, S.L. Zhu, Phys. Rep. **639**, 1 (2016). arXiv:1601.02092 [hep-ph]
3. L. Tang, C.F. Qiao, Eur. Phys. J. C **76**, 558 (2016). arXiv:1603.04761 [hep-ph]
4. W. Chen, H.X. Chen, X. Liu, T.G. Steele, S.L. Zhu, Phys. Rev. Lett. **117**, 022002 (2016). arXiv:1602.08916 [hep-ph]

5. F. Stancu, J. Phys. G **43**, 105001 (2016). arXiv:1603.03322 [hep-ph]
6. Y.R. Liu, X. Liu, S.L. Zhu, Phys. Rev. D **93**, 074023 (2016). arXiv:1603.01131 [hep-ph]
7. C.M. Zanetti, M. Nielsen, K.P. Khemchandani, Phys. Rev. D **93**, 096011 (2016). arXiv:1602.09041 [hep-ph]
8. J.M. Dias, K.P. Khemchandani, A.A. Martínez Torres, M. Nielsen, C.M. Zanetti, Phys. Lett. B **758**, 235 (2016). arXiv:1603.02249 [hep-ph]
9. Z.G. Wang, Commun. Theor. Phys. **66**, 335 (2016). arXiv:1602.08711 [hep-ph]
10. Z.G. Wang, Eur. Phys. J. C **76**, 279 (2016). arXiv:1603.02498 [hep-ph]
11. S.S. Agaev, K. Azizi, H. Sundu, Phys. Rev. D **93**, 074024 (2016). arXiv:1602.08642 [hep-ph]
12. S.S. Agaev, K. Azizi, H. Sundu, Eur. Phys. J. Plus **131**, 351 (2016). arXiv:1603.02708 [hep-ph]
13. S.S. Agaev, K. Azizi, H. Sundu, Phys. Rev. D **93**, 114007 (2016). arXiv:1603.00290 [hep-ph]
14. Q.F. Lü, Y.B. Dong, Phys. Rev. D **94**, 094041 (2016). arXiv:1603.06417 [hep-ph]
15. X.H. Liu, G. Li, Eur. Phys. J. C **76**, 455 (2016). arXiv:1603.00708 [hep-ph]
16. C.J. Xiao, D.Y. Chen, arXiv:1603.00228 [hep-ph]
17. T.J. Burns, E.S. Swanson, Phys. Lett. B **760**, 627 (2016). arXiv:1603.04366 [hep-ph]
18. F.K. Guo, U.-G. Meißner, B.S. Zou, Commun. Theor. Phys. **65**, 593 (2016). arXiv:1603.06316 [hep-ph]
19. X. Chen, J. Ping, Eur. Phys. J. C **76**, 351 (2016). arXiv:1604.05651 [hep-ph]
20. W. Wang, R. Zhu, Chin. Phys. C **40**, 093101 (2016). arXiv:1602.08806 [hep-ph]
21. R. Aaij et al., LHCb Collaboration, Phys. Rev. Lett. **117**, 152003 (2016). arXiv:1608.00435 [hep-ex]
22. CMS Collaboration, CMS-PAS-BPH-16-002 (2016)
23. W.A. Bardeen, E.J. Eichten, C.T. Hill, Phys. Rev. D **68**, 054024 (2003). arXiv:hep-ph/0305049
24. E.E. Kolomeitsev, M.F.M. Lutz, Phys. Lett. B **582**, 39 (2004). arXiv:hep-ph/0307133
25. F.K. Guo, P.N. Shen, H.C. Chiang, R.G. Ping, B.S. Zou, Phys. Lett. B **641**, 278 (2006). arXiv:hep-ph/0603072
26. M. Cleven, F.K. Guo, C. Hanhart, U.-G. Meißner, Eur. Phys. J. A **47**, 19 (2011). arXiv:1009.3804 [hep-ph]
27. L. Liu, K. Orginos, F.K. Guo, C. Hanhart, U.-G. Meißner, Phys. Rev. D **87**, 014508 (2013). arXiv:1208.4535 [hep-lat]
28. M. Altenbuchinger, L.S. Geng, W. Weise, Phys. Rev. D **89**, 014026 (2014). arXiv:1309.4743 [hep-ph]
29. S.S. Agaev, K. Azizi, H. Sundu, Phys. Rev. D **93**, 094006 (2016). arXiv:1603.01471 [hep-ph]
30. Z.H. Guo, U.-G. Meißner, D.L. Yao, Phys. Rev. D **92**, 094008 (2015). arXiv:1507.03123 [hep-ph]
31. D.L. Yao, M.L. Du, F.K. Guo, U.-G. Meißner, JHEP **1511**, 058 (2015). arXiv:1502.05981 [hep-ph]
32. M. Albaladejo, J. Nieves, E. Oset, Z.F. Sun, X. Liu, Phys. Lett. B **757**, 515 (2016). arXiv:1603.09230 [hep-ph]
33. X.W. Kang, J.A. Oller, Phys. Rev. D **94**, 054010 (2016). arXiv:1606.06665 [hep-ph]
34. C.B. Lang, D. Mohler, S. Prelovsek, Phys. Rev. D **94**, 074509 (2016). arXiv:1607.03185 [hep-lat]
35. M. Altenbuchinger, L.S. Geng, Phys. Rev. D **89**, 054008 (2014). arXiv:1310.5224 [hep-ph]
36. D. Gamermann, E. Oset, D. Strottman, M.J. Vicente, Vacas. Phys. Rev. D **76**, 074016 (2007). arXiv:hep-ph/0612179
37. D. Gamermann, E. Oset, Eur. Phys. J. A **33**, 119 (2007). arXiv:0704.2314 [hep-ph]
38. J.X. Lu, Y. Zhou, H.X. Chen, J.J. Xie, L.S. Geng, Phys. Rev. D **92**, 014036 (2015). arXiv:1409.3133 [hep-ph]
39. A. Ozpineci, C.W. Xiao, E. Oset, Phys. Rev. D **88**, 034018 (2013). arXiv:1306.3154 [hep-ph]
40. C.B. Lang, D. Mohler, S. Prelovsek, R.M. Woloshyn, Phys. Lett. B **750**, 17 (2015). arXiv:1501.01646 [hep-lat]
41. Y. Zhou, X.L. Ren, H.X. Chen, L.S. Geng, Phys. Rev. D **90**, 014020 (2014). arXiv:1404.6847 [nucl-th]
42. S. Weinberg, Phys. Rev. **130**, 776 (1963)
43. S. Weinberg, Phys. Rev. **137**, B672 (1965)
44. C. Hanhart, Y.S. Kalashnikova, A.V. Nefediev, Phys. Rev. D **81**, 094028 (2010). arXiv:1002.4097 [hep-ph]
45. V. Baru, J. Haidenbauer, C. Hanhart, Y. Kalashnikova, A.E. Kudryavtsev, Phys. Lett. B **586**, 53 (2004). arXiv:hep-ph/0308129
46. M. Cleven, F.K. Guo, C. Hanhart, U.-G. Meißner, Eur. Phys. J. A **47**, 120 (2011). arXiv:1107.0254 [hep-ph]
47. D. Gamermann, J. Nieves, E. Oset, E. Ruiz Arriola, Phys. Rev. D **81**, 014029 (2010). arXiv:0911.4407 [hep-ph]
48. J. Yamagata-Sekihara, J. Nieves, E. Oset, Phys. Rev. D **83**, 014003 (2011). arXiv:1007.3923 [hep-ph]
49. F. Aceti, E. Oset, Phys. Rev. D **86**, 014012 (2012). arXiv:1202.4607 [hep-ph]
50. C.W. Xiao, F. Aceti, M. Bayar, Eur. Phys. J. A **49**, 22 (2013). arXiv:1210.7176 [hep-ph]
51. F. Aceti, L.R. Dai, L.S. Geng, E. Oset, Y. Zhang, Eur. Phys. J. A **50**, 57 (2014). arXiv:1301.2554
52. F. Aceti, E. Oset, L. Roca, Phys. Rev. C **90**, 025208 (2014). arXiv:1404.6128 [hep-ph]
53. T. Hyodo, D. Jido, A. Hosaka, Phys. Rev. C **85**, 015201 (2012). arXiv:1108.5524 [nucl-th]
54. T. Hyodo, Int. J. Mod. Phys. A **28**, 1330045 (2013). arXiv:1310.1176 [hep-ph]
55. I. Sekihara, I. Hyodo, D. Jido, PTEP **2015**, 063D04 (2015). arXiv:1411.2308 [hep-ph]
56. H. Nagahiro, A. Hosaka, Phys. Rev. C **90**, 065201 (2014). arXiv:1406.3684 [hep-ph]
57. C. Garcia-Recio, C. Hidalgo-Duque, J. Nieves, L.L. Salcedo, L. Tolos, Phys. Rev. D **92**, 034011 (2015). arXiv:1506.04235 [hep-ph]
58. Z.H. Guo, J.A. Oller, Phys. Rev. D **93**, 096001 (2016). arXiv:1508.06400 [hep-ph]
59. L.S. Geng, X.L. Ren, Y. Zhou, H.X. Chen, E. Oset, Phys. Rev. D **92**, 014029 (2015). arXiv:1503.06633 [hep-ph]
60. V. Bernard, U.-G. Meißner, A. Rusetsky, Nucl. Phys. B **788**, 1 (2008). arXiv:hep-lat/0702012
61. X.L. Ren, L.S. Geng, J. Meng, Phys. Rev. D **89**, 054034 (2014). arXiv:1307.1896 [nucl-th]
62. L.S. Geng, X.L. Ren, J. Martin-Camalich, W. Weise, Phys. Rev. D **84**, 074024 (2011). arXiv:1108.2231 [hep-ph]
63. S. Aoki et al., PACS-CS Collaboration, Phys. Rev. D **79**, 034503 (2009). arXiv:0807.1661 [hep-lat]